Optimizing closed-loop adaptive-optics performance with use of multiple control bandwidths

Brent L. Ellerbroek

Starfire Optical Range, U.S. Air Force Phillips Laboratory, Kirtland Air Force Base, New Mexico 87117

Charles Van Loan and Nikos P. Pitsianis

Department of Computer Science, Cornell University, Ithaca, New York 14853

Robert J. Plemmons

Department of Mathematics and Computer Science, Wake Forest University, Winston-Salem, North Carolina 27109

Received February 17, 1994; revised manuscript received June 24, 1994; accepted June 24, 1994

The performance of a closed-loop adaptive-optics system may in principle be improved by selection of distinct and independently optimized control bandwidths for separate components, or modes, of the wave-front-distortion profile. We describe a method for synthesizing and optimizing a multiple-bandwidth adaptive-optics control system from performance estimates previously derived for single-bandwidth control systems operating over a range of bandwidths. The approach is applicable to adaptive-optics systems that use either one or several wave-front sensing beacons and also to systems that include multiple deformable mirrors for atmospheric-turbulence compensation across an extended field of view. Numerical results are presented for the case of an atmospheric-turbulence profile consisting of a single translating phase screen with Kolmogorov statistics, a Shack–Hartmann wave-front sensor with from 8 to 16 subapertures across the aperture of the telescope, and a continuous-face-sheet deformable mirror with actuators conjugate to the corners of the wave-front-sensor subapertures. The use of multiple control bandwidths significantly relaxes the wave-front-sensor noise level that is permitted for the adaptive-optics system to operate near the performance limit imposed by fitting error. Nearly all of this reduction is already achieved through the use of a control system that uses only two distinct bandwidths, one of which is the zero bandwidth.

1. INTRODUCTION

Closed-loop adaptive-optics systems must compensate for time-varying wave-front distortions on the basis of noisy sensor measurements. Time-varying distortions are most accurately corrected by a system with a high control bandwidth, but the noise in wave-front-sensor measurements is best rejected by reduction of the control bandwidth and temporal smoothing of the wave-front correction to be applied. These trends lead to a performance trade-off between the residual wave-front distortions that are due to sensor noise and servo lag, and the optimum control bandwidth that minimizes the sum of these two effects will depend on the wave-front-sensor noise level and the temporal characteristics of the wave-front errors to be corrected. Most adaptive-optics systems developed to date have addressed this trade-off through the use of a common control bandwidth for all components of the wave-front-distortion profile,[1–3] but systems employing several different control bandwidths for separate wave-front components have been studied[4–7] and recently tested in the atmosphere.[8–12] Because wave-front-sensor noise statistics and the temporal dynamics of the wave-front distortion to be corrected vary as a function of spatial frequency,[6,13] it should in principle be possible to improve adaptive-optics performance by using this more sophisticated control approach. In this paper we describe a technique for evaluating and optimizing the performance of adaptive-optics systems with use of multiple control bandwidths. We also compare the performance of the multiple and single-bandwidth control approaches for the case of atmospheric-turbulence compensation and a range of representative adaptive-optics system parameters.

One can readily achieve bandwidth optimization for a closed-loop adaptive-optics system, using a single bandwidth, by using standard results for the effects of sensor noise and servo lag on adaptive-optics performance. Since the wave-front errors that are due to these two effects may be treated as statistically independent, the combined mean-square phase error $\sigma^2(f)$ to be minimized by adjustment of the control bandwidth f takes the form

$$\sigma^2(f) = \sigma_n^2(f) + \sigma_s^2(f), \tag{1.1}$$

where the terms $\sigma_n^2(f)$ and $\sigma_s^2(f)$ are the mean-square phase errors that are due to sensor noise and servo lag. Explicit formulas for these two quantities depend on numerous parameters, including wave-front-distortion statistics, wave-front-sensor noise statistics, the geometries for the wave-front-sensor subapertures and the deformable-mirror actuators, the wave-front reconstruction algorithm, and the impulse response function of the adaptive-optics control loop.[14] The value of f that minimizes $\sigma^2(f)$ may be determined numerically, and analytical solutions may be obtained when scaling-law

0740-3232/94/112871-16$06.00

approximations are assumed for the functions $\sigma_n^2(f)$ and $\sigma_s^2(f)$.[15–18]

The performance of a modal adaptive-optics control system[5,19] may be improved further by application of the above optimization process separately to each distinct component, or mode, of the wave-front-distortion profile. For a system that uses an orthonormal basis of deformable-mirror profiles as the set of modes to be controlled, Eq. (1.1) is replaced by formulas of the form[5,6,12]

$$\sigma^2 = \sum_{i=1}^{N} \sigma_i^2(f_i), \tag{1.2}$$

$$\sigma_i^2(f_i) = (\sigma_i^2)_n(f_i) + (\sigma_i^2)_s(f_i), \tag{1.3}$$

where σ_i^2 is the mean-square residual phase error in mode number i, f_i is the control bandwidth for this mode, and $(\sigma_i^2)_n(f_i)$ and $(\sigma_i^2)_s(f_i)$ are the statistically independent contributions of sensor noise and servo lag, respectively, to the total mean-square phase error in mode number i. Explicit formulas for the latter two functions may be computed from wave-front-distortion statistics and adaptive-optics system parameters once an *a priori* basis of orthonormal control modes has been selected. The bandwidth f_i that minimizes Eq. (1.3) may then be determined numerically for each i. Zernike polynomials[20] are frequently used as the control-mode basis for analytical calculations, although practical applications require that this basis set be adjusted to match the influence-function characteristics of a particular deformable mirror.[5]

A basic limitation of the above approach is that the choice of the control-mode basis is external to the optimization process. Control bandwidths are determined after an *a priori* control-mode basis has been specified, and there is no way to vary both the control modes and their associated control bandwidths simultaneously to minimize more globally the mean-square phase error σ^2. There are evidently no analytical techniques yet available for incorporating the temporal dynamics of the phase distortions to be compensated into the definition of the wave-front control-mode basis set itself. This is especially true for adaptive-optics systems that use either multiple wave-front sensing beacons or several deformable mirrors to compensate for atmospheric turbulence accross an extended field of view.

In this paper we describe a technique for improving the performance of an adaptive-optics system by simultaneously optimizing both the basis of wave-front control modes and their associated control bandwidths. The inputs to this procedure are a collection of real, symmetric $n \times n$ matrices $\mathcal{M}^{(1)}, \ldots, \mathcal{M}^{(n_c)}$ that have been derived from the second-order statistics of single-bandwidth control systems for n_c different bandwidths that sample the bandwidth range of interest. The variable n denotes the number of deformable-mirror degrees of freedom. One optimizes adaptive-optics control modes and bandwidths by maximizing the functional $f(U) = \Sigma_{i=1}^{n} \max_{1<j\le n_c}\{(U^T \mathcal{M}^{(j)} U)_{ii}\}$ over all $n \times n$ unitary matrices U. The columns of the optimal U define the orthogonal basis of control modes in terms of deformable-mirror-actuator commands. Mode number i is controlled at bandwidth number k precisely when matrix $\mathcal{M}^{(k)}$ maximizes the quantity $(U^T \mathcal{M}^{(j)} U)_{ii}$ over $j = 1, \ldots, n_c$. The unitary U that maximizes $f(U)$ is computed with use of an iterative algorithm that is in some ways analogous to the Jacobi method for diagonalizing a symmetric matrix.[21] The optimal U may also be determined explicitly from the eigenvectors of $\mathcal{M}^{(1)}$ in the special case where $n_c = 2$ and $\mathcal{M}^{(2)} \equiv 0$, because the second of the two control bandwidths is the zero bandwidth. We refer to this special case as reduced-range single-bandwidth control, since the range of the wave-front reconstruction matrix is in this case a proper subspace of the vector space of deformable-mirror-actuator commands.

It is interesting to note that these techniques are applicable independently of the adaptive-optics system parameters and input disturbance characteristics that determine the matrices $\mathcal{M}^{(k)}$. These results are applicable to adaptive-optics configurations including multiple deformable mirrors and wave-front-sensing beacons, for example, and may also be used when matrices $\mathcal{M}^{(k)}$ include the effects of time-varying telescope misalignments or other disturbances that are distinct from atmospheric turbulence. One limitation of the approach is that control bandwidths are optimized over a finite set of discrete values, not over the continuum of all possible control bandwidths. For sample calculations with use of a Kolmogorov turbulence spectrum, we find that 10–20 distinct values are sufficient to sample the bandwidth range of interest fully. It is in principle possible first to select the basis of control modes and initial control bandwidth estimates with use of the techniques introduced in this paper and then to refine the control bandwidth values further by means of the standard approach summarized after Eqs. (1.2) and (1.3) above.

The remainder of the paper is organized as follows. Analytical results are derived in Section 2, beginning with a review of single-bandwidth adaptive-optics systems in Subsection 2.A. Subsection 2.B evaluates the performance of a multiple-bandwidth control system for a prespecified set of control modes and bandwidths. Subsection 2.C describes how the functional $f(U)$ may be used to optimize the performance of a multibandwidth adaptive-optics control system, and Subsection 2.D considers the special case of reduced-range single-bandwidth control. The results on closed-loop wave-front reconstruction obtained in a previous paper are equivalent to the material in this subsection.[22]

Sample numerical results are presented in Section 3. These results assume a single translating phase screen with Kolmogorov statistics, a Shack–Hartmann wave-front sensor with 8–16 subapertures across the telescope aperture diameter, and a continuous-face-sheet deformable mirror with actuator locations conjugate to the corners of the wave-front-sensing subapertures. Adaptive-optics performance is compared for adaptive-optics systems with use of a single optimized control bandwidth, multiple control bandwidths, or reduced-range single-bandwidth control. The use of multiple control bandwidths significantly relaxes the wave-front-sensor noise level that is permitted for an adaptive-optics system to operate near the performance limit imposed by fitting error. Nearly all of this reduction can be achieved through the use of reduced-range single-bandwidth control.

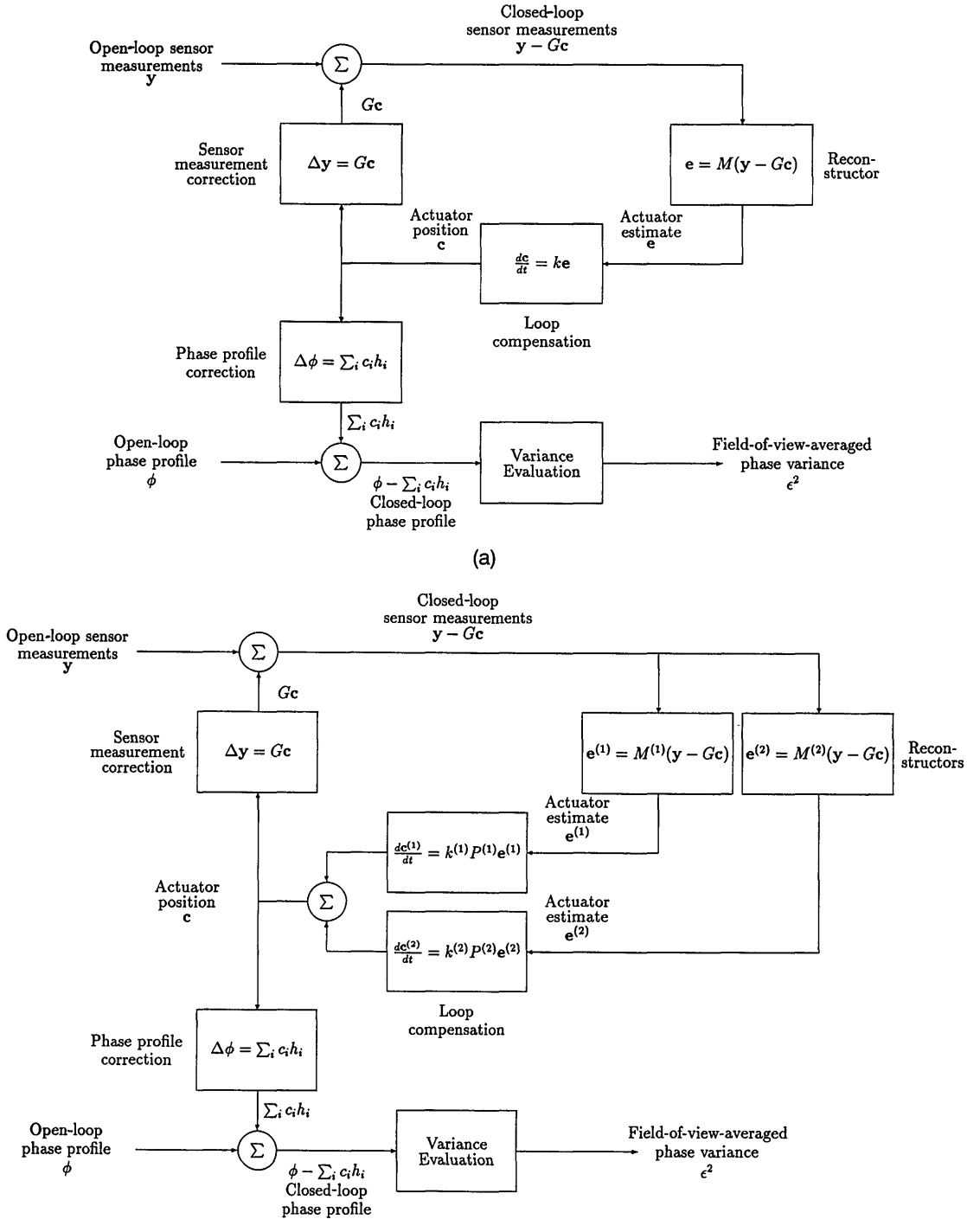

Fig. 1. Adaptive-optics system control-loop dynamics: (a) an adaptive-optics control system in which all wave-front modes are compensated at the same servo bandwidth; (b) a system that uses different bandwidths and estimation algorithms for distinct, orthogonal subspaces of wave-front modes. Only two separate bandwidths are illustrated for the sake of concreteness, but the approach may be generalized to any number of distinct control bandwidths.

Section 4 discusses the implications of these results for adaptive control concepts designed to adjust adaptive-optics control bandwidths in real time in response to variations in sensor noise level and wave-front-distortion dynamics. Appendix A summarizes the iterative algorithm that is used to maximize the functional $f(U)$ in the general case. Appendix B considers the special case of exactly two control bandwidths.

2. ANALYTICAL RESULTS

Figure 1 illustrates the closed-loop adaptive-optics control approaches to be investigated in this paper. Figure 1(a) is a block diagram of the single-control-bandwidth approach. The top two thirds of this figure represents the adaptive-optics control loop itself, and the bottom third describes the effect of the control system on the optical

performance of the telescope. Figure 1(b) illustrates an adaptive-optics control loop that employs multiple control bandwidths for separate modes, or components, of the overall wave-front-distortion profile. The control loops and the notation introduced in these figures are described further in the paragraphs below. Formulas for evaluating and optimizing the optical performance of these systems are then developed in the following subsections.

The input disturbance to be nulled by the control system is the time-varying m-dimensional vector $\mathbf{y}(t)$ of wave-front-slope sensor measurements. This vector can be composed of components obtained from one or several natural or artificial wave-front-sensing beacons that may be displaced from or coincident with the object to be imaged. The vector $\mathbf{y}(t)$ includes the effect of wave-front-sensor measurement noise but not the feedback applied to the sensor measurements by deformable-mirror-actuator adjustments. This second effect is included in the quantity $\mathbf{y}(t) - G\mathbf{c}(t)$, where $\mathbf{c}(t)$ is an n-dimensional vector composed of the deformable-mirror-actuator position commands at time t, and $G = \partial\mathbf{y}/\partial\mathbf{c}$ is the $m \times n$ Jacobian matrix of first-order changes in wave-front measurements $\mathbf{y}$ with respect to variations in the deformable-mirror-actuator command vector $\mathbf{c}$. The actuator command vector $\mathbf{c}$ may include commands for actuators on one or several deformable mirrors that are conjugate to different locations along the propagation path between the telescope and the scene to be imaged. Each component of the vector $\mathbf{c}$ may also correspond to a linear combination of commands to multiple physical actuators. It is convenient to assume that the null space of the matrix G contains only the zero vector, so that all nonzero actuator command vectors result in some effect on the wave-front-slope sensor measurement vector. This condition can be obtained by restriction of attention to a linear subspace of the space of all possible actuator command vectors if necessary.

The single-bandwidth control law that is used to determine deformable-mirror-actuator commands from the closed-loop wave-front-slope sensor measurement vector $\mathbf{y} - G\mathbf{c}$ is defined by the equations

$$\mathbf{e} = M(\mathbf{y} - G\mathbf{c}), \tag{2.1}$$

$$\frac{d\mathbf{c}}{dt} = k\mathbf{e}. \tag{2.2}$$

The $n \times m$ matrix M is referred to as the wave-front reconstruction matrix, and the vector $\mathbf{e}$ is the estimate of the instantaneous closed-loop wave-front distortion represented as a sum of deformable-mirror-actuator adjustments. Equation (2.2) relates the rate of change of the deformable-mirror-actuator command vector to the instantaneous wave-front-distortion estimate $\mathbf{e}$. Note that all components of the command vector $\mathbf{c}$ are driven at the same bandwidth by use of parallel single-input, single-output control laws. The particular form for this control law was selected for the sake of simplicity and concreteness. The methods to be developed below apply equally well to any control law described by a linear ordinary differential equation with constant coefficients.

The wave-front-distortion profile to be corrected by the adaptive-optics control loop is represented in Fig. 1(a) by the notation $\phi(\mathbf{r}, \theta)$ and is a function of both the point $\mathbf{r}$ in the telescope aperture plane at which it is evaluated and the direction θ in the field of view of the telescope from which the phase profile has propagated. Since the phase profile $\phi(\mathbf{r}, \theta)$ and any modified profile of the form $\phi(\mathbf{r}, \theta) + f(\theta)$ will have identical effects on the imaging performance of the telescope, it is convenient to assume that the function $\phi(\mathbf{r}, \theta)$ has been summed with a function of θ to satisfy the condition

$$\int d\mathbf{r} W_A(\mathbf{r})\phi(\mathbf{r}, \theta) \equiv 0, \tag{2.3}$$

where $W_A(\mathbf{r})$ is a $\{0, 1\}$-valued function describing the clear aperture of the telescope. The function $\phi(\mathbf{r}, \theta)$ that includes this mathematical adjustment will be referred to as a piston-removed phase profile. The adjustment $\Delta\phi(\mathbf{r}, \theta)$ applied to the phase profile by the adaptive-optics system is assumed to be a linear function of the actuator command vector $\mathbf{c}$ and is described by the equation

$$\Delta\phi(\mathbf{r}, \theta) = \sum_i c_i h_i(\mathbf{r}, \theta), \tag{2.4}$$

where each function $h_i(\mathbf{r}, \theta)$ is the adjustment to the phase profile that results when a unit command is applied to actuator number i. This influence function will depend on field angle θ when the actuator is located on a deformable mirror that is not conjugate to the aperture plane of the telescope. We will assume that the overall piston has been removed from each of these influence functions, so that Eq. (2.3) applies with $\phi(\mathbf{r}, \theta)$ replaced with $h_i(\mathbf{r}, \theta)$. Equation (2.4) will sometimes be abbreviated with operator notation in the form

$$\Delta\phi = H\mathbf{c}. \tag{2.5}$$

H is a linear operator by Eq. (2.4).

The optical performance of the adaptive-optics system is quantified by use of the expected mean-square value of the residual phase-distortion profile $\phi - \Delta\phi$. This mean-square residual phase error is expressed in terms of an inner product $[f, g]$ defined by the expression

$$[f, g] = \frac{\int d\mathbf{r} \int d\theta W_A(\mathbf{r}) W_F(\theta) f(\mathbf{r}, \theta) g(\mathbf{r}, \theta)}{\int d\mathbf{r} \int d\theta W_A(\mathbf{r}) W_F(\theta)}, \tag{2.6}$$

where f and g are real-valued functions of $\mathbf{r}$ and θ and W_F is a nonnegative function of θ that quantifies the relative weight attached to different points in the field of view of the telescope. This inner product is symmetric ($[f, g] = [g, f]$) and linear in both f and g. The expected mean-square residual phase error σ^2 is defined by the formula

$$\sigma^2 = \langle [\phi - \Delta\phi, \phi - \Delta\phi] \rangle, \tag{2.7}$$

where the angle brackets denote ensemble averaging over the statistics of random sensor noise and phase-distortion profiles $\phi(\mathbf{r}, \theta)$. The details of how these averages are numerically calculated for specific wave-front-sensor and

deformable-mirror configurations are described in previous studies.[22–24] For the present paper it suffices to note that ensemble averaging is a linear operation.

The following analysis is simplified if we assume that deformable-mirror-actuator commands are expressed in terms of a basis set satisfying the condition

$$[H\mathbf{c}, H\mathbf{c}'] = \mathbf{c}^T\mathbf{c}', \tag{2.8}$$

for any two actuator command vectors $\mathbf{c}$ and $\mathbf{c}'$. This is equivalent to the requirement that

$$[h_i, h_j] = \delta_{ij}, \tag{2.9}$$

where δ_{ij} is the Kronecker delta function. One may always obtain this condition by orthogonalizing any prespecified basis set of deformable-mirror-actuator commands. After this orthogonalization procedure, the basis elements of the deformable-mirror-actuator command vector $\mathbf{c}$ will correspond to linear combinations of multiple physical deformable-mirror actuators.

The multiple-bandwidth adaptive-optics control system illustrated in Fig. 1(b) replaces Eqs. (2.1) and (2.2) with the estimation and control law

$$\mathbf{e}^{(i)} = M^{(i)}(\mathbf{y} - G\mathbf{c}), \tag{2.10}$$

$$\frac{d\mathbf{c}^{(i)}}{dt} = k^{(i)}P^{(i)}\mathbf{e}^{(i)}, \tag{2.11}$$

$$\mathbf{c} = \sum_i \mathbf{c}^{(i)}. \tag{2.12}$$

The index i varies over the n_c different bandwidths employed by the adaptive-optics control loop. Once again, the particular loop compensation equation given in Eq. (2.11) is employed for the sake of simplicity and concreteness. The bandwidth $k^{(i)}$ is used for deformable-mirror adjustments within the range space of the orthogonal projection operator $P^{(i)}$, and the total correction applied to the deformable mirror is the sum of these separately computed components. The projection operators $P^{(i)}$ must satisfy the conditions

$$P^{(i)}P^{(i)} = P^{(i)}, \tag{2.13}$$

$$[P^{(i)}]^T = P^{(i)}, \tag{2.14}$$

$$P^{(i)}P^{(j)} = 0 \qquad \text{for } i \neq j, \tag{2.15}$$

$$\sum_i P^{(i)} = I. \tag{2.16}$$

Equations (2.13) and (2.14) are necessary and sufficient conditions for each matrix $P^{(i)}$ to be an orthogonal projection operator.[21,25] Equations (2.15) and (2.16) imply that the range spaces of these projections decompose the space of all deformable-mirror-actuator commands into mutually orthogonal linear subspaces. The multiple-bandwidth adaptive-optics system illustrated in Fig. 1(b) includes the previously described special case of modal control with use of a Zernike polynomial basis for deformable-mirror-actuator commands.[5]

With the above introduction it is now possible to evaluate and optimize the performance of these two adaptive-optics control approaches. Formulas for this purpose are developed in the following subsections.

A. Single-Bandwidth Systems

The steady-state solution to the single-bandwidth control law described by Eqs. (2.1) and (2.2) takes the form

$$\mathbf{c}(t) = \int_0^\infty d\tau k \exp(-k\tau MG)M\mathbf{y}(t - \tau). \tag{2.17}$$

The deformable-mirror-actuator command vector $\mathbf{c}(t)$ is a highly nonlinear function of the reconstruction matrix M, and either optimizing or evaluating adaptive-optics performance appears to be difficult in this general case. We therefore introduce the constraint

$$MG = I \tag{2.18}$$

on the coefficients of the matrix M. Equation (2.18) may be interpreted as requiring the reconstruction matrix to estimate precisely the current set of deformable-mirror-actuator commands in the absence of noise and atmospheric turbulence. Because the null space of the matrix G contains only the zero vector, one possible choice of M that satisfies Eq. (2.18) is the matrix $(G^TG)^{-1}G^T$.[21] Equation (2.18) does not uniquely specify the reconstruction matrix M, however, except in the highly unusual case in which there are equal numbers of wave-front-slope sensor measurements and deformable-mirror actuators.

Substituting Eq. (2.18) back into Eq. (2.17) gives the formula

$$\mathbf{c}(t) = M\mathbf{s}(t), \tag{2.19}$$

where the temporally filtered wave-front-slope measurement vector is defined as

$$\mathbf{s}(t) = \int_0^\infty d\tau k \exp(-k\tau)\mathbf{y}(t - \tau). \tag{2.20}$$

The deformable-mirror-actuator command vector $\mathbf{c}(t)$ is now a linear function of the coefficients of the wave-front reconstruction matrix M. If Eq. (2.2) were replaced by another linear differential equation with scalar-valued, constant coefficients, Eq. (2.20) for $\mathbf{s}(t)$ would become the corresponding steady-state solution with zero initial conditions.

A formula for the expected mean-square residual phase error σ^2 can now be obtained by substitution of Eqs. (2.5) and (2.19) back into Eq. (2.7). This yields the result

$$\sigma^2 = \langle[\phi - HM\mathbf{s}, \phi - HM\mathbf{s}]\rangle. \tag{2.21}$$

With use of the linearity and symmetry properties of the inner product operator, Eq. (2.21) may be expanded into the form

$$\sigma^2 = \langle[\phi, \phi]\rangle - 2\sum_{i,j}\langle[\phi, h_i]s_j\rangle M_{ij} + \sum_{i,j,i',j'}[h_i, h_{i'}]M_{ij}M_{i'j'}\langle s_j s_{j'}\rangle. \tag{2.22}$$

We note that the term $\langle[\phi, \phi]\rangle$ is finite for the case of turbulence-induced phase profiles with Kolmogorov statistics, because the function ϕ has been defined as the

piston-removed component of the wave-front-distortion profile. Introducing the standard definitions[23,24]

$$\sigma_0^2 = \langle [\phi, \phi] \rangle, \tag{2.23}$$

$$A_{ij} = \langle [\phi, h_i] s_j \rangle, \tag{2.24}$$

$$S_{jj'} = \langle s_j s_{j'} \rangle \tag{2.25}$$

and applying the orthogonality condition for h_i given by Eq. (2.9) permit this expression for σ^2 to be simplified to the form

$$\begin{aligned}\sigma^2 &= \sigma_0^2 - 2\sum_{i,j} A_{ij}M_{ij} + \sum_{i,j,j'} M_{ij}M_{ij'}S_{jj'} \\ &= \sigma_0^2 - \mathrm{tr}(AM^T) - \mathrm{tr}(MA^T) + \mathrm{tr}(MSM^T),\end{aligned} \tag{2.26}$$

where $\mathrm{tr}(V)$ denotes the trace of a square matrix V. This is the desired formula for the optical performance of a single-bandwidth adaptive-optics control loop. Computational formulas for numerically evaluating the statistical quantities σ_0^2, A, and S for the case of Kolmogorov turbulence have been described previously.[22]

The formula for the expected mean-square residual phase distortion is quadratic in the coefficients of the reconstruction matrix M, and the constraints imposed upon M by Eq. (2.18) are linear. The value of M that minimizes the error σ^2 may therefore be determined with use of Lagrange multipliers. The result is the expression

$$M = AS^{-1} + (I - AS^{-1}G)(G^TS^{-1}G)^{-1}G^TS^{-1}. \tag{2.27}$$

The first term in this formula for M is the usual minimum-variance reconstructor without constraints,[23,24] and the second term is the adjustment necessary for satisfying the constraint imposed by Eq. (2.18).[26] The spatial and temporal statistics of the phase-distortion profile to be corrected influence the value of the reconstruction matrix M through the covariance matrices S and A. The minimum expected mean-square residual phase error for a single-bandwidth adaptive-optics control loop at the bandwidth k may be determined by substitution of this value of M back into Eq. (2.26). After algebraic simplifications, the formula for σ^2 becomes

$$\begin{aligned}\sigma^2 = \sigma_0^2 &- \mathrm{tr}(AS^{-1}A^T) \\ &+ \mathrm{tr}[(I - AS^{-1}G)(G^TS^{-1}G)^{-1}(I - G^TS^{-1}A^T)].\end{aligned} \tag{2.28}$$

In analogy to Eq. (2.27), the first two terms in this formula can be recognized as the usual result for the performance of an unconstrained minimum-variance reconstructor.[23,24]

B. Evaluating Multiple-Bandwidth Systems

The first step in evaluating the performance of a multiple-bandwidth adaptive-optics control loop is to derive an expression for the actuator command vector $\mathbf{c}(t)$ equivalent to Eq. (2.19) in the single-bandwidth case. We will once again assume a constraint of the form

$$M^{(i)}G = I \tag{2.29}$$

for each of the reconstruction matrices $M^{(i)}$, although the particular value of this matrix does not have to be derived with use of the results of Subsection 2.A. The derivation of a formula for $\mathbf{c}(t)$ begins with the identity

$$\begin{aligned}\frac{\mathrm{d}}{\mathrm{d}t}[P^{(i)}\mathbf{c}] &= P^{(i)}\frac{\mathrm{d}\mathbf{c}}{\mathrm{d}t} \\ &= \sum_j P^{(i)}\frac{\mathrm{d}\mathbf{c}^{(j)}}{\mathrm{d}t},\end{aligned} \tag{2.30}$$

where the second equality follows from Eq. (2.12). With use of Eqs. (2.10), (2.11), and (2.29), Eq. (2.30) becomes

$$\frac{\mathrm{d}}{\mathrm{d}t}[P^{(i)}\mathbf{c}] = k^{(i)}P^{(i)}M^{(i)}\mathbf{y} - k^{(i)}P^{(i)}\mathbf{c}, \tag{2.31}$$

where all terms of the summation may be dropped except for $i = j$ on account of Eq. (2.15). The steady-state solution to this differential equation takes the form

$$P^{(i)}\mathbf{c}(t) = \int_0^\infty \mathrm{d}\tau k^{(i)} \exp[-k^{(i)}\tau]P^{(i)}M^{(i)}\mathbf{y}(t - \tau). \tag{2.32}$$

Introducing the definition

$$\mathbf{s}^{(i)}(t) = \int_0^\infty \mathrm{d}\tau k^{(i)} \exp[-k^{(i)}\tau]\mathbf{y}(t - \tau) \tag{2.33}$$

permits this solution to be abbreviated as the formula

$$P^{(i)}\mathbf{c}(t) = P^{(i)}M^{(i)}\mathbf{s}^{(i)}(t). \tag{2.34}$$

Summing Eq. (2.34) over i and applying Eq. (2.16) give the result

$$\mathbf{c}(t) = \sum_i P^{(i)}M^{(i)}\mathbf{s}^{(i)}(t), \tag{2.35}$$

which is the desired formula for the deformable-mirror-actuator command vector $\mathbf{c}(t)$. This solution is simply the sum of contributions from the individual wave-front reconstruction matrices $M^{(i)}$ on the range spaces of the projection operators $P^{(i)}$, and there is no cross coupling among the separate reconstructors. This simplification would not have been obtained without Eq. (2.15).

A formula for the expected mean-square residual phase distortion of the multiple-bandwidth adaptive-optics system may now be obtained by substitution of Eqs. (2.5) and (2.35) into Eq. (2.7). This gives the result

$$\sigma^2 = \left\langle \left[\phi - \sum_i HP^{(i)}M^{(i)}\mathbf{s}^{(i)}, \phi - \sum_i HP^{(i)}M^{(i)}\mathbf{s}^{(i)} \right] \right\rangle, \tag{2.36}$$

which may be expanded to become the expression

$$\begin{aligned}\sigma^2 = \sigma_0^2 &- 2\sum_{i,j,k} \langle [\phi, h_j] s_k^{(i)} \rangle [P^{(i)}M^{(i)}]_{jk} \\ &+ \sum_{i,j,k,i',j',k'} [h_j, h_{j'}][P^{(i)}M^{(i)}]_{jk}[P^{(i')}M^{(i')}]_{j'k'}\langle s_k^{(i)} s_{k'}^{(i')} \rangle.\end{aligned} \tag{2.37}$$

Introducing the definitions

$$A_{jk}^{(i)} = \langle [\phi, h_j] s_k^{(i)} \rangle, \tag{2.38}$$

$$S_{kk'}^{(ii')} = \langle s_k^{(i)} s_{k'}^{(i')} \rangle, \tag{2.39}$$

and applying the orthogonality condition for h_i given in Eq. (2.9) yield the result

$$\sigma^2 = {\sigma_0}^2 - 2 \sum_{i,j,k} A_{jk}^{(i)} [P^{(i)} M^{(i)}]_{jk} + \sum_{i,i',j,k,k'} [P^{(i)} M^{(i)}]_{jk} [P^{(i')} M^{(i')}]_{jk'} S_{kk'}^{(ii')} \tag{2.40}$$

for the value of the expected mean-square residual phase error σ^2. The sums over j, k, and k' in this expression may be rewritten in the form

$$\sigma^2 = {\sigma_0}^2 - \sum_i \mathrm{tr}\{P^{(i)} M^{(i)} [A^{(i)}]^T\} - \sum_i \mathrm{tr}\{A^{(i)} [M^{(i)}]^T [P^{(i)}]^T\} + \sum_{i,i'} \mathrm{tr}\{P^{(i)} M^{(i)} S^{(ii')} [M^{(i')}]^T [P^{(i')}]^T\}. \tag{2.41}$$

Because the identity

$$\mathrm{tr}(MN) = \mathrm{tr}(NM) \tag{2.42}$$

is valid whenever the product MN is a square matrix, Eqs. (2.13)–(2.15) may be substituted into Eq. (2.41) for the quantity σ^2 to yield

$$\sigma^2 = {\sigma_0}^2 - \sum_i \mathrm{tr}\big(P^{(i)}\{M^{(i)}[A^{(i)}]^T + A^{(i)}[M^{(i)}]^T - M^{(i)} S^{(ii)} [M^{(i)}]^T\} P^{(i)}\big). \tag{2.43}$$

The definition

$$\mathcal{M}^{(i)} = M^{(i)}[A^{(i)}]^T + A^{(i)}[M^{(i)}]^T - M^{(i)} S^{(ii)} [M^{(i)}]^T \tag{2.44}$$

allows this expression for σ^2 to be rewritten in the form

$$\sigma^2 = {\sigma_0}^2 - \sum_i \mathrm{tr}(P^{(i)} \mathcal{M}^{(i)} P^{(i)}). \tag{2.45}$$

This is the desired formula for the expected mean-square residual phase distortion for a multiple-bandwidth adaptive-optics control loop.

We note for use below that matrix $\mathcal{M}^{(i)}$ is symmetric. It follows from the definitions of matrices $A^{(i)}$ and $S^{(ii)}$ that $\mathcal{M}^{(i)}$ satisfies the relationship

$$\mathcal{M}_{jk}^{(i)} = \langle [h_j, \phi][h_k, \phi] \rangle - \langle [h_j, \phi - HM^{(i)}\mathbf{s}^{(i)}] \times [h_k, \phi - HM^{(i)}\mathbf{s}^{(i)}] \rangle. \tag{2.46}$$

Matrix $\mathcal{M}^{(i)}$ describes the change to the second-order statistics of the correctable component of the phase-distortion profile that results when the reconstruction matrix $M^{(i)}$ and the control bandwidth $k^{(i)}$ are employed in a single-bandwidth adaptive-optics control loop. Equation (2.45) then illustrates the relationship between the overall performance of the multiple-bandwidth control loop and the performance of the individual reconstruction matrices and bandwidths from which it is constructed. We note once again that there is no cross coupling among different reconstruction algorithms in this formula and that this condition would not be obtained without Eqs. (2.13)–(2.15).

C. Optimizing Multiple-Bandwidth Systems

Suppose now that the single-bandwidth reconstruction algorithms $M^{(i)}$ have been optimized with use of Eq. (2.27) for a range of control bandwidths $k^{(i)}$ and that the corresponding matrices $\mathcal{M}^{(i)}$ defined by Eq. (2.44) have been computed. We assume that the sampled values of $k^{(i)}$ represent the range of control bandwidths that are possibly of interest for the given adaptive-optics parameters and operating conditions. How can we determine orthogonal projection operators $P^{(i)}$ that will optimize the performance of the resulting multiple-bandwidth adaptive-optics control loop? More precisely, we are interested in determining the value of the minimum expected mean-square residual phase distortion ${\sigma_*}^2$ defined by the formula

$${\sigma_*}^2 = \min\left\{ {\sigma_0}^2 - \sum_i \mathrm{tr}[P^{(i)} \mathcal{M}^{(i)} P^{(i)}] : [P^{(1)}, \ldots, P^{(n_c)}] \in \mathcal{P} \right\} = {\sigma_0}^2 - \max\left\{ \sum_i \mathrm{tr}[P^{(i)} \mathcal{M}^{(i)} P^{(i)}] : [P^{(1)}, \ldots, P^{(n_c)}] \in \mathcal{P} \right\}, \tag{2.47}$$

where the set $\mathcal{P}$ is the collection of sequences of matrices $[P^{(1)}, \ldots, P^{(n_c)}]$ satisfying Eqs. (2.13)–(2.16). The maximum in Eq. (2.47) is taken over both the bandwidths at which modes are controlled and the control modes themselves. This approach is more general than is selecting optimal control bandwidths for each mode in a preselected basis set, such as Zernike polynomials. The value of ${\sigma_*}^2$ obtained will therefore be less than or equal to the best performance achievable with a prespecified basis set and the same range of allowable control bandwidths.

The goal of this subsection is to obtain an equivalent formula for ${\sigma_*}^2$ in which the maximization operator is applied over a set that is more easily characterized than $\mathcal{P}$. Every sequence $[P^{(1)}, \ldots, P^{(n_c)}]$ that is an element of $\mathcal{P}$ may be written in the form

$$P^{(i)} = U \Lambda^{(i)} U^T, \tag{2.48}$$

where the matrix U is a unitary matrix,

$$UU^T = U^T U = I, \tag{2.49}$$

and the diagonal matrices $\Lambda^{(i)}$ satisfy the conditions

$$\Lambda^{(i)} = \mathrm{diag}[\lambda_1^{(i)}, \ldots, \lambda_n^{(i)}], \tag{2.50}$$

$$\lambda_j^{(i)} = 0 \text{ or } 1, \tag{2.51}$$

$$\sum_i \Lambda^{(i)} = I. \tag{2.52}$$

One constructs the columns of matrix U by combining orthonormal basis sets for the range spaces of each $P^{(i)}$. One defines the diagonal matrices $\Lambda^{(i)}$ by setting $\lambda_j^{(i)}$ equal to unity if column number j of U is within the range space of $P^{(i)}$ and equal to zero otherwise. Equations (2.13)–(2.16) ensure that U is unitary and

that Eq. (2.52) is satisfied. Conversely, any sequence of matrices constructed with use of Eqs. (2.48)–(2.52) will satisfy Eqs. (2.13)–(2.16) and therefore will be an element of the set $\mathcal{P}$. This equivalency and Eq. (2.42) permit the definition of $\sigma_*{}^2$ to be rewritten as

$$\sigma_*{}^2 = \sigma_0{}^2 - \max\left\{\sum_i \mathrm{tr}[\Lambda^{(i)} U^T \mathcal{M}^{(i)} U) : U \text{ unitary}, [\Lambda^{(1)}, \ldots, \Lambda^{(n_c)}] \in \mathcal{L}\right\}, \quad (2.53)$$

where $\mathcal{L}$ is the collection of sequences of diagonal matrices satisfying Eqs. (2.50)–(2.52).

For fixed U the maximum over $\mathcal{L}$ in Eq. (2.53) takes the value

$$\max\left\{\sum_i \mathrm{tr}[\Lambda^{(i)} U^T \mathcal{M}^{(i)} U] : [\Lambda^{(1)}, \ldots, \Lambda^{(n_c)}] \in \mathcal{L}\right\} = \sum_{j=1}^{n} \max_i [U^T \mathcal{M}^{(i)} U]_{jj}, \quad (2.54)$$

where this maximum is achieved for $[\Lambda^{(1)}, \ldots, \Lambda^{(n_c)}]$, given by the prescription

$$\lambda_j^{(i)} = \begin{cases} 1 & \text{if } [U^T \mathcal{M}^{(i)} U]_{jj} = \max_k [U^T \mathcal{M}^{(k)} U]_{jj} \\ 0 & \text{otherwise} \end{cases}. \quad (2.55)$$

Substituting Eq. (2.54) back into Eq. (2.53) yields the formula

$$\sigma_*{}^2 = \sigma_0{}^2 - \max\left\{\sum_{j=1}^{n} \max_i [U^T \mathcal{M}^{(i)} U]_{jj} : U \text{ unitary}\right\}, \quad (2.56)$$

for the value of the minimum expected mean-square residual phase distortion achievable with a multiple-bandwidth adaptive-optics control loop. The columns of the unitary matrix U that is associated with this minimum become the control modes for the optimal control algorithm. Mode number j is controlled by use of bandwidth $k^{(i)}$ precisely when $[U^T \mathcal{M}^{(i)} U]_{jj} = \max_k [U^T \mathcal{M}^{(k)} U]_{jj}$.

Several theoretical and practical considerations must be addressed before Eq. (2.56) can be viewed as a feasible approach to selecting control modes and control bandwidths for a closed-loop adaptive-optics system. Does a unitary matrix U that minimizes σ^2 necessarily exist, and is it unique? Is there a unitary U that will minimize σ^2 over the entire continuous range of control bandwidths? Can the value of $\sigma_*{}^2$ so achieved be approached to arbitrary precision by means of optimization over sufficiently dense finite sets of bandwidths? Finally, is there a practical algorithm for finding a value for U that minimizes Eq. (2.56) for any prespecified value of n_c and any set of matrices $\mathcal{M}^{(1)}, \ldots, \mathcal{M}^{(n_c)}$? We consider the theoretical questions first.

The set of $n \times n$ unitary matrices is a compact set for the standard topology defined by the Hilbert–Schmidt norm. The right-hand side of Eq. (2.56) is a continuous function of U with respect to this topology for any fixed set of matrices $\mathcal{M}^{(1)}, \ldots, \mathcal{M}^{(n_c)}$; and continuous, real-valued functions defined on compact sets always achieve their minimum and maximum values. Therefore a value of U that actually minimizes σ^2 in Eq. (2.56) always exists. This matrix U is not necessarily unique, since more than one value of U will correspond to the same set of projection operators $P^{(1)}, \ldots, P^{(n_c)}$ in Eq. (2.47) whenever the range space of at least one of these projections is more than one dimensional. This condition appears to be consistently obtained whenever matrices A, S, and G contain symmetries arising from x–y-symmetric deformable mirrors and wave-front sensors. Multiple values of U associated with a common set of projections $P^{(1)}, \ldots, P^{(n_c)}$ in Eq. (2.47) do, however, yield the same multiple-bandwidth control algorithm. The uniqueness or nonuniqueness of the multiple-bandwidth control algorithm yielding the minimum value of σ^2 in Eq. (2.56) must depend on properties of matrices $\mathcal{M}^{(1)}, \ldots, \mathcal{M}^{(n_c)}$ that we have not attempted to characterize.

Consider now how the value of $\sigma_*{}^2$ achieved in Eq. (2.56) varies as the number and range of control bandwidths included in the optimization increases toward infinity. For any particular adaptive-optics system, the set of bandwidths k of interest is restricted to a bounded range $[0, K]$ by practical considerations (such as the finite speed of light). From Eqs. (2.20), (2.24), and (2.25) it follows that the covariance matrices S and A are continuous functions of the bandwidth k of a single-bandwidth adaptive-optics control loop. Owing to Eqs. (2.27) and (2.46), the matrices M and $\mathcal{M}^{(k)}$ are similarly continuous in k, where (for the remainder of this subsection only) the matrices $\mathcal{M}^{(k)}$ are now parameterized directly in terms of the bandwidth k. It follows that the function $g_j(U, k)$ defined by the expression

$$g_j(U, k) = [U^T \mathcal{M}^{(k)} U]_{jj} \quad (2.57)$$

is continuous on the product space of pairs of $n \times n$ unitary matrices and bandwidths k from the interval $[0, K]$. This domain is compact, so the functions are in fact uniformly continuous. The functions $\max_{0 \le k \le K} [U^T \mathcal{M}^{(k)} U]_{jj}$ and $\Sigma_{j=1}^{n} \max_{0 \le k \le K} [U^T \mathcal{M}^{(k)} U]_{jj}$ are therefore continuous in U and must achieve their maximum value on the compact set of $n \times n$ unitary matrices. It follows that there exists a unitary matrix U_* that minimizes the mean-square residual phase error,

$$\sigma^2 = \sigma_0{}^2 - \sum_{j=1}^{n} \max_{0 \le k \le K} [U^T \mathcal{M}^{(k)} U]_{jj}, \quad (2.58)$$

over all possible definitions of wave-front control modes (or unitary matrices U) and control bandwidths selected from the range $[0, K]$.

The performance of the continuously optimized solution obtained above may be approximated to arbitrary precision by means of optimization over sufficiently dense finite sets of bandwidths. Since each function $g_j(U, k)$ is uniformly continuous, for every positive ϵ there exists a positive δ such that $\|U - U'\| < \delta$ and $|k - k'| < \delta$ imply that $|g_j(U, k) - g_j(U', k')| < \epsilon/n$ for $j = 1, \ldots, n$. If the finite set of bandwidths $\{k_1, \ldots, k_{n_c}\}$ is selected so that all bandwidths k in the range $[0, K]$ satisfy $|k - k_i| < \delta$ for some i, it follows that

$$\max_{0 \le k \le K} [U^T \mathcal{M}^{(k)} U]_{jj} \le \max_i [U^T \mathcal{M}^{(k_i)} U]_{jj} + \epsilon/n \quad (2.59)$$

for all unitary matrices U and j, with $1 \le j \le n$. Summing over j and maximizing over U yields the desired result, namely,

$$\max_U \sum_{j=1}^{N} \max_{0\le k\le K} [U^T \mathcal{M}^{(k)} U]_{jj} \le \max_U \sum_{j=1}^{N} \max_i [U^T \mathcal{M}^{(k_i)} U]_{jj} + \epsilon . \quad (2.60)$$

Quantitative bounds on convergence rates (i.e., the required values for δ and n_c as functions of the desired ϵ) are beyond the scope of this paper. Numerical results in Section 3 below will illustrate how we have selected n_c and the bandwidth bound K for a sample problem.

We now consider the more practical question, finding the optimal unitary U in Eq. (2.56) for a given value of n_c and prespecified matrices $\mathcal{M}^{(1)}, \ldots, \mathcal{M}^{(n_c)}$. We have not found a practical closed-form solution to this problem. The objective function σ^2 is not differentiable with respect to U, and the collection $\{[U, \sigma^2(U)] : U \text{ unitary}\}$ is not a convex set. Our approach to approximating $\sigma_*{}^2$ for sample numerical problems uses a pairwise, iterative optimization procedure somewhat analogous to the Jacobi method for diagonalizing a symmetric matrix. The details of this hill-climbing search algorithm are described in Appendix A. Although the convergence (termination) of the search is guaranteed, we do not know whether the maximum reached is global. Several reasons for confidence in the practical utility of this method for numerical calculations are described below in Section 3.

D. Reduced-Range Single-Bandwidth Systems

The simplest possible multiple-bandwidth control system employs one nonzero and one zero control bandwidth. In the present notation this system is described by the parameters

$$n_c = 2, \quad (2.61)$$

$$k^{(1)} = k, \quad (2.62)$$

$$k^{(2)} = 0. \quad (2.63)$$

With $k^{(2)} = 0$ it follows quickly from the definitions given in Eqs. (2.33), (2.38), (2.39), and (2.44) that

$$\mathbf{s}^{(2)} = 0, \quad (2.64)$$

$$A^{(2)} = 0, \quad (2.65)$$

$$S^{(22)} = 0, \quad (2.66)$$

$$\mathcal{M}^{(2)} = 0, \quad (2.67)$$

so that Eq. (2.56) for the minimum expected mean-square residual phase distortion becomes

$$\sigma_*{}^2 = \sigma_0{}^2 - \max\left\{ \sum_{j=1}^{n} \max[(U^T \mathcal{M} U)_{jj}, 0] : U \text{ unitary} \right\} . \quad (2.68)$$

Because matrix $\mathcal{M}$ is symmetric, it may be written with an eigenvalue/eigenvector decomposition of the form

$$\mathcal{M} = U_0 D U_0{}^T, \quad (2.69)$$

where U_0 is unitary and $D = \mathrm{diag}(d_1, \ldots, d_n)$ is diagonal. The formula for $\sigma_*{}^2$ consequently becomes

$$\sigma_*{}^2 = \sigma_0{}^2 - \max\left\{ \sum_{j=1}^{n} \max[(U^T U_0 D U_0{}^T U)_{jj}, 0] : U \text{ unitary} \right\} . \quad (2.70)$$

It is intuitively plausible that the maximum in Eq. (2.70) is achieved for the value of U that diagonalizes $\mathcal{M}$, namely, $U = U_0$; this result is proven in Appendix B. The formula for $\sigma_*{}^2$ therefore simplifies to the closed-form solution

$$\sigma_*{}^2 = \sigma_0{}^2 - \sum_{j=1}^{n} \max(d_j, 0) . \quad (2.71)$$

The control modes associated with this minimum are simply the eigenvectors of $\mathcal{M}$, and a given mode is corrected at nonzero bandwidth precisely when the associated eigenvalue is positive. This expression recovers an earlier result for the optimal range space of a wave-front reconstruction algorithm for systems that use a single nonzero control bandwidth.[22]

3. NUMERICAL RESULTS

In this section we apply the above analytical results to representative cases of atmospheric-turbulence compensation. The atmospheric-turbulence profile considered consists of a single thin phase screen $\phi(\mathbf{r}, \theta) \equiv \phi(\mathbf{r})$ in the aperture plane of the telescope, with a structure function of the form

$$\langle |\phi(\mathbf{r}) - \phi(\mathbf{r} + \mathbf{r}')|^2 \rangle = 6.88 \left(\frac{r'}{r_0} \right)^{5/3}, \quad (3.1)$$

where r_0 is the turbulence-induced atmospheric coherence diameter. This structure function corresponds to a Kolmogorov turbulence spectrum with an infinite outer scale and zero inner scale. The temporal dynamics of the phase screen are given by the Taylor hypothesis,

$$\phi(\mathbf{r}, t) = \phi(\mathbf{r} - t\mathbf{v}, 0), \quad (3.2)$$

where t represents time and $\mathbf{v}$ is a constant wind-velocity vector. The windspeed v is assumed to be known, and separate results are presented for the two cases in which the direction of $\mathbf{v}$ is either known or unknown and is uniformly distributed. For the case of a single translating phase screen, the definition for the Greenwood frequency f_g that is used to describe the temporal bandwidth of turbulence-induced phase distortions simplifies to the relationship[18]

$$f_g = 0.423 v / r_0 . \quad (3.3)$$

The adaptive-optics systems considered consist of a Shack–Hartmann wave-front sensor and a continuous-face-sheet deformable mirror. The dimensionality of the system is parameterized by the ratio D/d, where D is the diameter of the circular, unobscured telescope aperture and d is the width of an individual wave-front-sensor

Table 1. Dimensionality of the Adaptive-Optics Systems Considered

System Component	D/d[a] 8	12	16
Fully illuminated subapertures	32	88	164
Partially illuminated subapertures	28	44	60
Total subapertures	60	132	224
Actuators in pupil	49	113	197
Edge actuators	28	44	60
Total actuators	77	157	257

[a] D, diameter of the circular, unobscured telescope aperture; d, width of a single subaperture in the Shack–Hartmann wave-front sensor. Deformable-mirror actuators are located conjugate to the corners of the wave-front-sensor subapertures in the Fried actuator/subaperture geometry.

subaperture. The cases $D/d = 8$, 12, and 16 have been evaluated, and details on the dimensionality of these three cases are summarized in Table 1. Partially illuminated subapertures and actuators outside of but coupling into the telescope aperture have been included in the analysis.

Shack–Hartmann-sensor measurements were modeled as x and y gradients of the wave-front-distortion profile averaged over the illuminated portions of each subaperture. The wave-front-sensor temporal sampling rate was assumed to be sufficiently large to support the highest control bandwidth of interest. Measurement noise was treated as uncorrelated, temporally white for each individual subaperture, and uncorrelated between separate subapertures. Wave-front-sensor measurement noise is parameterized by the quantity σ_n^2, defined as the mean-square phase-difference measurement error for a fully illuminated subaperture and a sensor sampling rate equal to ten times the Greenwood frequency. The mean-square sensor noise for partially illuminated subapertures and other sampling rates was assumed to vary linearly with the sampling rate and inversely with the area of the subaperture. These sample dependencies imply that detector noise can be neglected as a source of wave-front-sensor measurement error and that $d \leq r_0$. Different scaling laws could be substituted to model the effects of noisy detectors or larger subapertures.

The deformable-mirror-actuator influence functions were modeled as linear splines with their widths equal to twice the interactuator spacing. Actuators were located conjugate to the corners of each wave-front-sensor subaperture in the so-called Fried geometry.[15]

Given the above assumptions, the performance of a single-bandwidth adaptive-optics system with use of an optimized wave-front reconstruction algorithm is fully determined by the size of the aperture, the strength of the turbulence, the Greenwood frequency of the turbulence, the control-loop bandwidth $f = k/(2\pi)$, and the wave-front-sensor noise variance σ_n^2 at the nominal sampling rate of $10f_g$. By inspection of Eqs. (2.26) and (2.27), the minimized mean-square residual phase error σ^2 is a function of the open-loop mean-square phase error σ_0^2, the covariance matrices A and S, and the Jacobian matrix G of first-order derivatives of wave-front-sensor measurements with respect to deformable-mirror-actuator adjustments. Numerical values for matrices A and S may be computed with Eqs. (3.18)–(3.28) of Ref. 22. Using these formulas and the above assumptions, we may show that these four quantities take the functional form

$$\sigma_0^2 = \left(\frac{d}{r_0}\right)^{5/3} 1.0299 \left(\frac{D}{d}\right)^{5/3}, \tag{3.4}$$

$$G = G\left(\frac{D}{d}\right), \tag{3.5}$$

$$A = \left(\frac{d}{r_0}\right)^{5/3} A_0\left(\frac{D}{d}, \frac{f_g r_0}{fd}\right), \tag{3.6}$$

$$\begin{aligned} S &= \left(\frac{d}{r_0}\right)^{5/3} S_0\left(\frac{D}{d}, \frac{f_g r_0}{fd}\right) + \sigma_n^2 \left(\frac{f}{f_g}\right) S_1\left(\frac{D}{d}\right) \\ &= \left(\frac{d}{r_0}\right)^{5/3} \left[S_0\left(\frac{D}{d}, \frac{f_g r_0}{fd}\right) \right. \\ &\quad \left. + \frac{\sigma_n^2}{(d/r_0)^{8/3}} \left(\frac{f_g r_0}{fd}\right)^{-1} S_1\left(\frac{D}{d}\right) \right]. \end{aligned} \tag{3.7}$$

By Eq. (3.3) the quantity $(f_g r_0)/(fd)$ is proportional to the fraction of a wave-front-sensor subaperture traversed by the translating phase screen in one servo time constant. The normalized quantities S_0 and S_1 are the separate, uncorrelated contributions of atmospheric-turbulence and wave-front-sensor noise to the covariance matrix S of temporally filtered sensor measurements. With use of Eqs. (2.26) and (2.27) and the above functional forms, it follows that the mean-square residual phase error σ^2 for an optimized single-bandwidth adaptive-optics system satisfies a scaling law of the form

$$\frac{\sigma^2}{(d/r_0)^{5/3}} = e^2\left(\frac{D}{d}, \frac{f_g r_0}{fd}, \frac{\sigma_n}{(d/r_0)^{4/3}}\right). \tag{3.8}$$

The normalized mean-square phase-error e^2 is a function of three quantities that may be interpreted as a normalized aperture diameter, a normalized servo lag, and a normalized wave-front-sensor noise level. When one is applying this scaling law it is important to note that, owing to Eq. (3.3), both variables f_g and σ_n^2 depend on the values of r_0 and d. These dependencies must be accounted for when one is comparing the performance of systems with different subaperture sizes.

Figure 2 plots the normalized mean-square residual phase error e^2 as a function of the normalized servo lag and the normalized wave-front-sensor noise level for the case $D/d = 8$ and a single-bandwidth adaptive-optics system when an optimized wave-front reconstructor is used. The direction of the wind is random and unknown. The results obtained are qualitatively similar to those of previous trade studies on this subject.[12] The best performance is naturally obtained for the case of no wave-front-sensor noise, and in this case the residual mean-square phase error decreases monotonically with decreasing servo lag toward an asymptote imposed by the effect of fitting error. For each of the four nonzero noise levels considered, there is an optimum control bandwidth that minimizes the combined effect of servo lag and sensor noise. The curves for the residual phase variance do not follow the idealized $(f_g/f)^{5/3}$ dependence for large values of (f_g/f) primarily because the telescope aperture diameter is finite.[27]

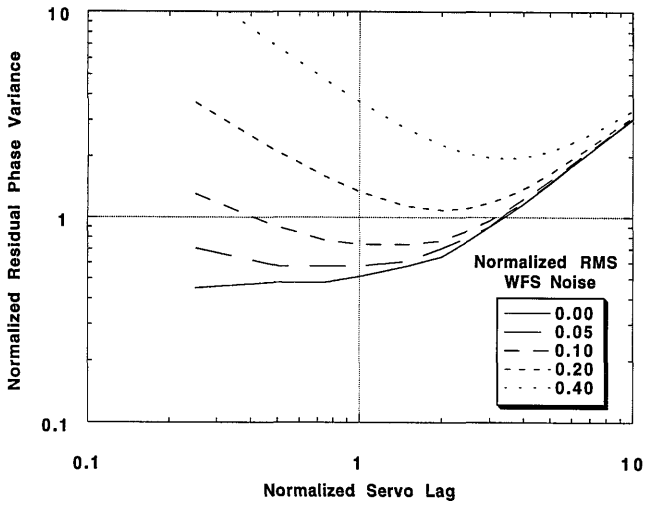

Fig. 2. Performance of an adaptive-optics control system with use of a single control bandwidth, as a function of normalized noise level and normalized servo lag. These results were obtained with use of the results described in Subsection 2.A. The results in this figure assume $D/d = 8$ and an unknown and random direction for the wind. The normalized residual phase variance is $\sigma^2/(d/r_0)^{5/3}$, the normalized servo lag is $(f_g r_0)/(fd)$, and the normalized root-mean-square (RMS) wave-front-sensor noise is defined as $\sigma_n/[2\pi(d/r_0)^{4/3}]$. The factor 2π is included in this definition so that the noise level is expressed in terms of waves when $d/r_0 = 1$. WFS, wave-front-sensor.

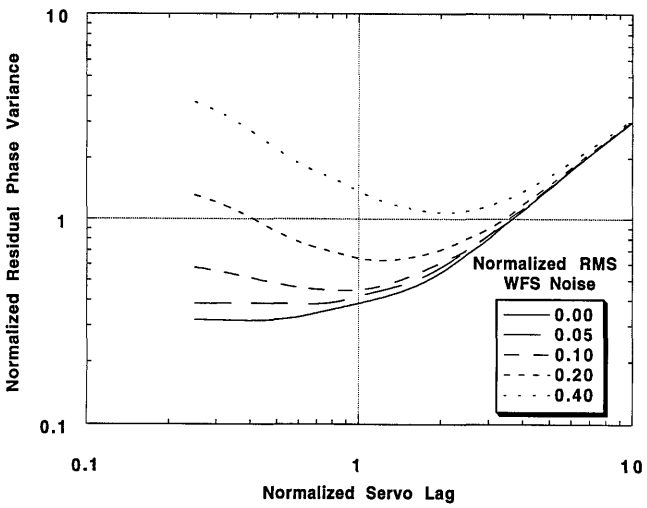

Fig. 3. Performance of an adaptive-optics control system with use of reduced-range single-bandwidth control as a function of normalized noise level and servo lag. These results correspond to those illustrated in Fig. 2, except that they assume the use of a reduced-range single-bandwidth control system as described in Subsection 2.D. WFS, wave-front-sensor.

Figure 3 plots comparable results for the performance of an adaptive-optics system with use of reduced-range single-bandwidth control. We computed these results by using Eq. (2.71) of Subsection 2.D. Simply not attempting to control those modes that are poorly sensed for a given level of wave-front-sensor noise and degree of servo lag yields a significant reduction in the mean-square residual phase error. For a given control loop bandwidth, the RMS wave-front-sensor noise level corresponding to a specified mean-square residual phase error is consistently at least doubled through the use of reduced-range single-bandwidth control. Some improvement is obtained even for the case of no wave-front sensor noise or a very small normalized servo lag. This result occurs because there are a small number of high-spatial-frequency modes that are poorly sensed because of aperture edge effects and that should not be controlled regardless of the control bandwidth or wave-front-sensor noise level.

Table 2 lists corresponding results for a multiple-bandwidth control system optimized as described in Appendix A over a set of 18 different control bandwidths yielding normalized servo lag values of 0.25–10. The precise bandwidths used are listed in the notes to Table 2 and are identical to the values evaluated for the single-bandwidth and the reduced-range single-bandwidth results plotted in Figs. 2 and 3, respectively. Because these sample numerical results are intended to be primarily illustrative, we performed no additional calculations to quantify how the results obtained depend on the value of n_c that we used and the exact bandwidths that we considered. The authors think that the results in Table 2 are near the limit for optimization over the continuum of all possible bandwidths, judging from the smoothness of the curves and location of the minima in Figs. 2 and 3.

Figure 4 compares the performance of the three different control options as a function of normalized noise level. The curve for the multiple-bandwidth control system is taken directly from Table 2. The curves for the single-bandwidth and the reduced-range single-bandwidth systems derived from the minima of the curves plotted in Figs. 2 and 3, so that the single bandwidths used for this comparison have been optimized as a function of the normalized wave-front-sensor noise level. The multiple-bandwidth and the reduced-range single-bandwidth approaches provide nearly identical performance improvements over the single-bandwidth control system. The significance of this improvement depends on which axis of Fig. 4 is considered the independent variable. The reduction in the mean-square phase error for a fixed sensor noise level is never greater than a factor of 2, but the relative change in the RMS sensor noise level permitted for a given mean-square residual phase error can

Table 2. Performance of a Multiple-Bandwidth Adaptive-Optics Control System as a Function of Wave-Front-Sensor Noise with $D/d = 8$ and a Random Wind Direction[a]

	Normalized Wave-Front-Sensor Noise				
	0.00	0.05	0.10	0.20	0.40
Normalized mean-square error	0.316	0.369	0.449	0.636	1.069

[a]The normalized wave-front-sensor noise level is defined as $\sigma_n/[2\pi(d/r_0)^{4/3}]$, and the normalized mean-square error is $\sigma^2/(d/r_0)^{5/3}$. σ_n is the RMS wave-front-sensor phase-difference measurement error in radians for a fully illuminated subaperture and a sampling rate equal to ten times the Greenwood frequency, d is the subaperture width, r_0 is the turbulence-induced coherence diameter, and σ^2 is the residual mean-square phase error for the multiple-bandwidth adaptive-optics control system computed with the methods described in Subsections 2.B and 2.C. A factor of 2π is included in the definition of the normalized noise level so that this quantity is expressed in terms of waves when $d/r_0 = 1$. The 18 different bandwidths used for constructing the multiple-bandwidth control algorithm correspond to normalized servo lags of 0.25, 0.50, 0.75, 1.00, 1.50, 2.00, 2.50, 3.00, 3.50, 4.00, 4.50, 5.00, 6.00, 7.00, 8.00, 9.00, 10.00, and ∞ (i.e., a control bandwidth of 0).

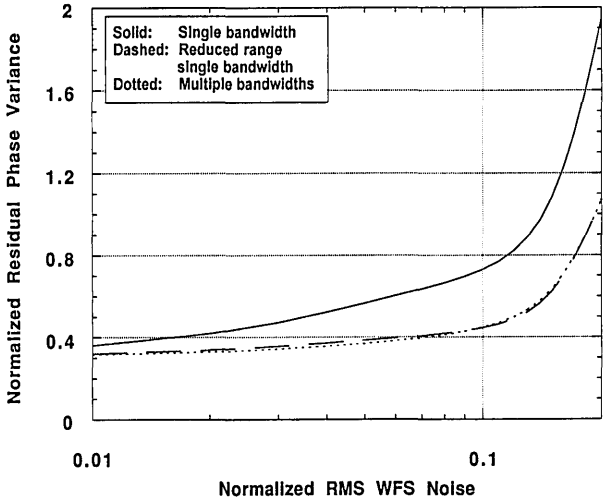

Fig. 4. Performance comparison of single-bandwidth control, reduced-range single-bandwidth control, and multiple-bandwidth control for $D/d = 8$ and a random wind direction. The multiple-bandwidth control results are taken from Table 2. The single-bandwidth and the reduced-range single-bandwidth results are the minima of the curves plotted in Figs. 2 and 3, respectively. The definitions for normalized residual phase variance and normalized RMS wave-front-sensor noise are as in Fig. 2. WFS, wave-front-sensor.

Table 3. Distribution of Modal Control Bandwidths for the Multiple-Bandwidth Control Results Given in Table 2[a]

Normalized Servo Lag	Normalized Noise Level 0.00	0.05	0.10	0.20	0.40
0.25	72	11	—	—	—
0.50	—	56	12	—	—
0.75	—	4	48	6	—
1.00	—	—	10	29	—
1.50	—	1	1	29	8
2.00	—	—	—	4	24
2.50	—	—	—	—	15
3.00	1	—	—	—	7
3.50	—	—	—	2	3
4.00	—	—	—	—	—
4.50	—	—	—	—	2
5.00	—	—	—	—	—
6.00	—	—	—	—	2
∞	3	4	5	6	15

[a]The definitions for normalized noise level and servo lag are as given in the caption for Fig. 2. Each column of the table lists the number of modes controlled at each bandwidth for the indicated normalized wave-front-sensor noise level. The row labeled ∞ is the number of modes left entirely uncontrolled by the bandwidth optimization process. Bandwidths corresponding to normalized servo lags of 7, 8, 9, and 10 were included in the optimization but were never selected. The total number of modes is 76 for each case.

be a considerably larger factor. The intensity required for the wave-front-sensing beacon would vary inversely with the square of the allowable RMS noise level in the case of a photon-limited wave-front sensor. For a sensor limited by either background noise or detector read noise, the required intensity would vary with the inverse of the RMS wave-front-sensor noise level.

Because the performances of the multiple-bandwidth and the reduced-range single-bandwidth approaches are so similar, it might be expected that the two control algorithms themselves would be approximately the same. One measure of their degree of similarity is given by Table 3, which lists the numerical distribution of bandwidths selected for the multiple-bandwidth control approach at the five different wave-front-sensor noise levels evaluated for Table 2. The sets of nonzero control bandwidths selected for the three lowest sensor noise levels are clustered tightly around the optimal bandwidths for the reduced-range single-bandwidth algorithm, as indicated by Fig. 3. The bandwidths utilized for the two highest sensor noise levels are more widely distributed, and the optimal reduced-range single-bandwidth solution is at most an engineering approximation to the multiple-bandwidth approach.

At this point it must be stressed that the multiple-bandwidth performance estimates presented in Table 2 and Fig. 4 are the results of the iterative hill-climbing optimization method described in Appendix A and that there is no mathematical certainty that these values are necessarily close to the global minima for the set of sample cases considered. It is at the least interesting to note, however, that (a) the performance of the multiple-bandwidth control algorithm as optimized by this approach is consistently very slightly superior to the reduced-range single-bandwidth approach for both this sample problem and all others that have been considered, (b) according to Table 3 the multiple-bandwidth control algorithms themselves are relatively close to the reduced-range single-bandwidth solutions, and (c) the multiple-bandwidth performance estimates in Fig. 4 were computed with a different random starting point for the iterative optimization procedure for each separate wave-front-sensor noise level listed in Table 2. A number of these cases were evaluated several times beginning with different random initial conditions, and the separate estimates for the normalized mean-square residual phase error varied by amounts of the order of 1.0×10^{-6}. All these points would certainly be grounds for additional investigation if the results in Table 2 were found to be significantly different from the actual global minima for the multiple-bandwidth control approach.

The results in Figs. 2–4 and Table 2 all assume that $D/d = 8$ and that the direction of the wind is random and unknown. Figure 5 presents results for a range of normalized aperture diameters D/d and both unknown and known wind directions.[28] The performance advantage afforded by either multiple-bandwidth control or reduced-range single-bandwidth control is smaller for $D/d = 12$ or 16 than for $D/d = 8$ and appears to have reached an asymptote. The results obtained are effectively independent of the wind model for a fixed value of D/d, although there is a very slight performance advantage associated with the use of the multiple-bandwidth approach when the wind direction is known. In no case are the results for multiple-bandwidth control and the reduced-range single-bandwidth control significantly different.

Because the present analysis has modeled the temporal dynamics of atmospheric turbulence with use of the Taylor hypothesis, it may be somewhat surprising that *a priori* knowledge of the wind direction has such a small effect on adaptive-optics performance. Wave-front modes evolve into linear combinations of other modes as the phase-distortion profile translates across the aper-

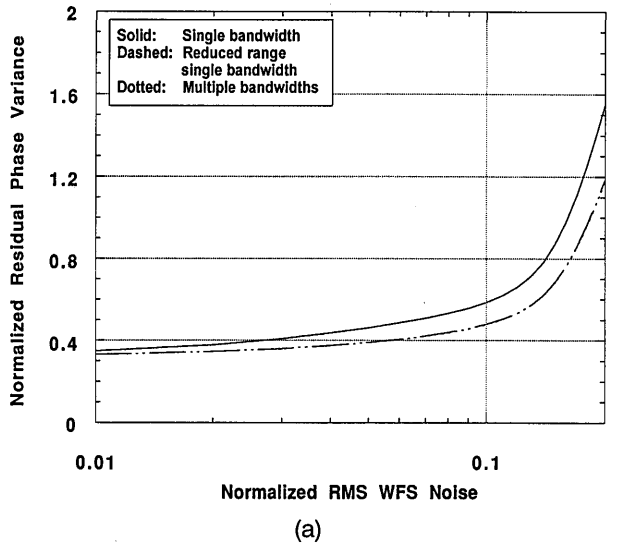

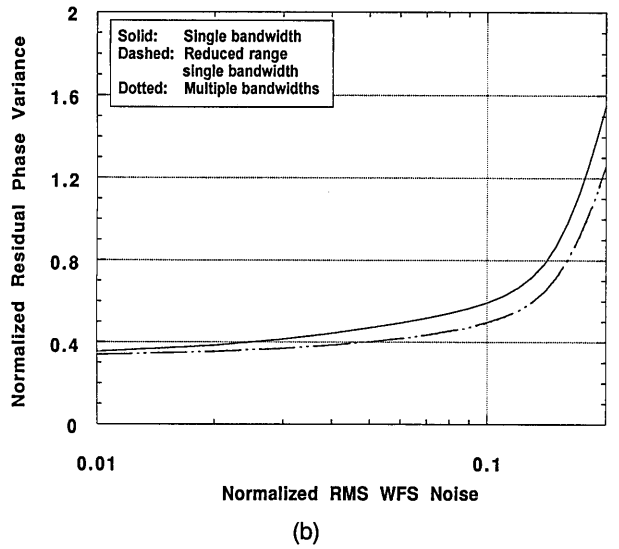

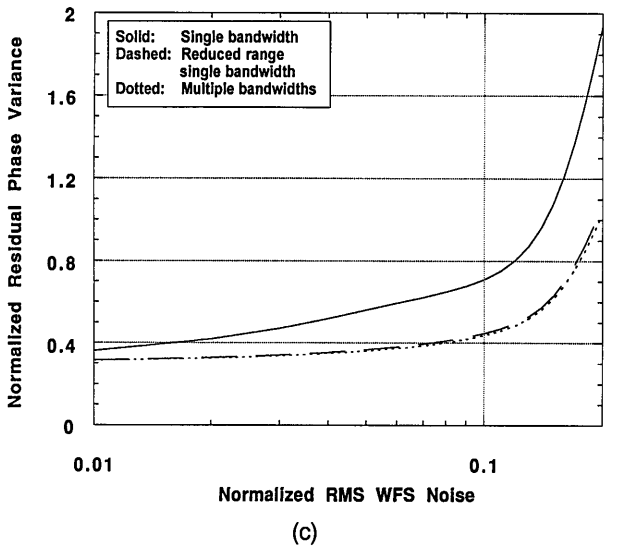

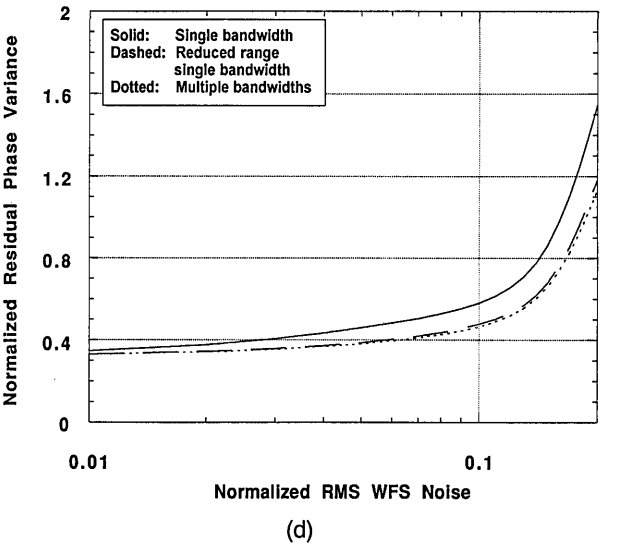

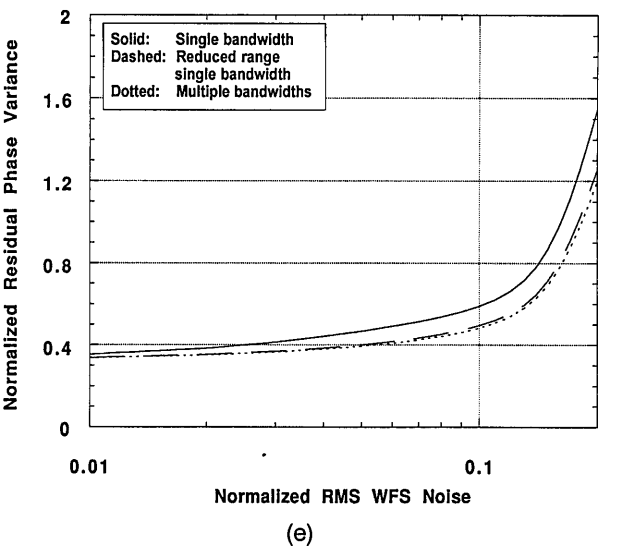

Fig. 5. Performance comparison of single-bandwidth control, reduced-range single-bandwidth control, and multiple-bandwidth control for different normalized aperture diameters and wind models. These plots are similar to those of Fig. 4, except that each subfigure describes results for a different normalized aperture diameter (D/d) and wind condition (known or unknown direction). (a) $D/d = 12$, random wind direction; (b) $D/d = 16$, random wind direction; (c) $D/d = 8$, known wind direction; (d) $D/d = 12$, known wind direction; (e) $D/d = 16$, known wind direction. WFS, wave-front-sensor.

ture, and a control algorithm must account for this cross coupling to exploit the predictability associated with the Taylor hypothesis. None of the three algorithms considered here satisfies this requirement. Figure 6 plots the mean-square phase distortion in each wave-front control mode for the multiple-bandwidth control approach both before and after correction and for unknown and known wind directions. The normalized aperture di-

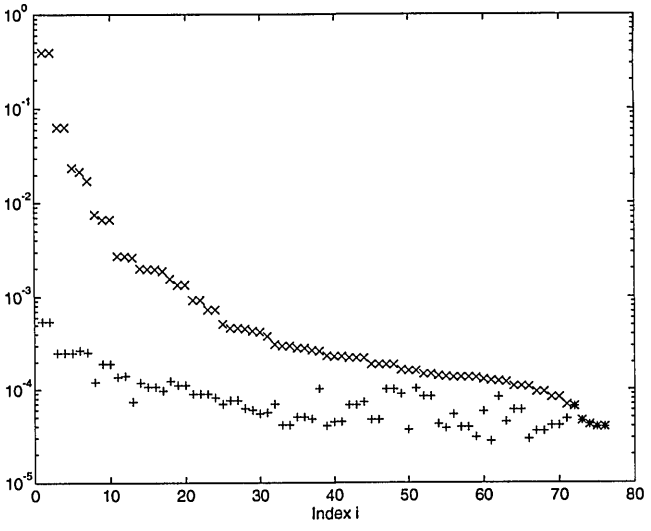

(a)

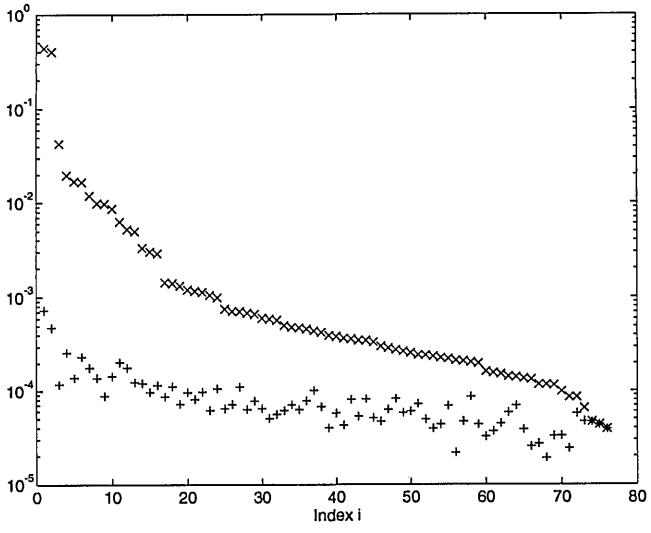

(b)

Fig. 6. Modal distribution of wave-front errors before (x) and after (+) compensation by the multiple-bandwidth control algorithm. These plots are for the normalized aperture diameter $D/d = 8$ and a normalized wave-front-sensor noise level of 0.1 wave at a sampling rate of ten times the Greenwood frequency. (a) Unknown wind direction, (b) known wind direction.

ameter is $D/d = 8$, and the normalized wave-front-sensor noise level is 0.1 wave at a sampling rate of ten times the Greenwood frequency. The values of the residual mean-square phase errors frequently come in pairs for the case of a random wind direction. This is consistent with the x–y symmetry of the wave-front-sensor subaperture geometry and the deformable-mirror-actuator geometry. The values of the residual errors do not occur in pairs and are much more scattered for a known wind direction, but their range and average value remain approximately the same.

4. DISCUSSION

This paper has described a technique for improving the performance of a modal adaptive-optics control system by simultaneously optimizing both the basis of wave-front control modes and their associated control bandwidths. A special case of this technique yields a control system that uses only a single bandwidth on a reduced range of the possible deformable-mirror degrees of freedom. The two approaches yield nearly identical performance improvements relative to an adaptive-optics control system that uses a single control bandwidth for all observable deformable-mirror degrees of freedom with an optimized wave-front reconstruction algorithm. These results apply for either a known wind direction or a wind direction that is both unknown and random. This lack of dependence on wind direction could simplify the implementation of adaptive control systems that are intended to adjust automatically for varying atmospheric conditions. It may also prove simpler to adjust a single nonzero control bandwidth in real time than to optimize an entire set of control bandwidths simultaneously.

Practical considerations may modify the above observations. All deformable-mirror degrees of freedom must be controlled by use of at least a low bandwidth to avoid drift resulting from hysteresis and roundoff error. Secondary mirror misalignments that are due to wind buffeting and line-of-sight acceleration introduce significant focus and astigmatism errors that may actually require higher control bandwidths for these low-order Zernike modes. It would also be interesting to see whether the results of this study apply to higher-order control laws and less-classical control architectures.

APPENDIX A: MAXIMIZING $F(U)$ (GENERAL CASE)

Given n_c $n \times n$ real symmetric matrices $\mathcal{M}^{(1)}$, $\mathcal{M}^{(2)}, \ldots, \mathcal{M}^{(n_c)}$, we want to find a unitary matrix U that maximizes the function

$$f(U) = \sum_{i=1}^{n} \max_{1 \le k \le n_c} \{[U^T \mathcal{M}^{(k)} U]_{ii}\}. \tag{A1}$$

A. Two-Matrix Algorithm

Let $n_c = 2$, $F = \mathcal{M}^{(1)}$, and $G = \mathcal{M}^{(2)}$. Suppose that the unitary matrix U with columns $u_1 \quad u_2 \quad \ldots \quad u_n$ is the maximizer. Without loss of generality the columns of U can be ordered in such a way that Eq. (A1) can be written as

$$f(U) = \sum_{i=1}^{r} u_i{}^T F u_i + \sum_{i=r+1}^{n} u_i{}^T G u_i, \tag{A2}$$

where r is the number of the diagonal elements of the product $U^T F U$ that are larger than the corresponding diagonal elements of $U^T G U$. Let $U = [U_1 | U_2]$, with $U_1 = [u_1 \quad u_2 \quad \ldots \quad u_r]$. Since U is unitary, it follows that

$$U U^T = U_1 U_1{}^T + U_2 U_2{}^T = I.$$

Using this expression and the trace properties

$$\mathrm{tr}(MN) = \mathrm{tr}(NM), \qquad \mathrm{tr}(M + N) = \mathrm{tr}(M) + \mathrm{tr}(N),$$

we can rewrite Eq. (A2) as follows:

$$\begin{aligned} f(U) &= \mathrm{tr}(U_1{}^T F U_1) + \mathrm{tr}(U_2{}^T G U_2) \\ &= \mathrm{tr}(F U_1 U_1{}^T) + \mathrm{tr}(G U_2 U_2{}^T) \\ &= \mathrm{tr}(F U_1 U_1{}^T) + \mathrm{tr}[G(I - U_1 U_1{}^T)] \\ &= \mathrm{tr}(F U_1 U_1{}^T) + \mathrm{tr}(G - G U_1 U_1{}^T) \\ &= \mathrm{tr}(F U_1 U_1{}^T - G U_1 U_1{}^T) + \mathrm{tr}(G) \\ &= \mathrm{tr}[(F - G) U_1 U_1{}^T] + \mathrm{tr}(G) \\ &= \mathrm{tr}[U_1{}^T (F - G) U_1] + \mathrm{tr}(G). \end{aligned}$$

Therefore in maximizing $f(U)$ the best we can do is to maximize the term $\mathrm{tr}[U_1{}^T(F - G)U_1]$ by taking as U_1 the eigenvectors of $F - G$ that correspond to positive eigenvalues; for a proof see Appendix B. This computation involves the Schur decomposition of the symmetric matrix $F - G$. For a description of the Schur decomposition algorithm see Ref. 21.

B. General Approach

With the two-matrix maximization algorithm we can solve the general n_c-matrix problem with a Jacobi-like approach. If M is an $n \times n$ matrix and s is a subset of the integers from 1 to n, we use the notation $M(s, s)$ to denote the submatrix of M with rows and columns in s. $M(:, s)$ denotes the submatrix with columns in s.

Let $U = U_0$ (an initial guess).
While the sequence is not converged, do the following:
  Let $B^{(k)}$ be $U^T \mathcal{M}^{(k)} U$ for all $k = 1 \ldots n_c$.
  Choose a pair of matrices $B^{(l)}$, $B^{(m)}$.
  Let u be the set of indices i such that either $B^{(l)}(i, i)$ or $B^{(m)}(i, i)$ is the maximum element over all $B^{(k)}(i, i)$ for $k = 1 \ldots n_c$.
  Let U_1 be the optimizer of the two-matrix subproblem $B^{(l)}(u, u)$, $B^{(m)}(u, u)$.
  Update $U(:, u)$ with $U(:, u)U_1$.

Since $\mathcal{M}^{(k)}$ is symmetric, the submatrix $\mathcal{M}^{(k)}(u, u)$ is symmetric for any set of indices u. The two-matrix subproblem contains the current maximum elements for the indices in u, so for any increase in the value of the sum of the maximum diagonal elements there will be at least as big an increase in the value of $f(U)$. That means that the sequence of matrices $\{U^{(k)}\}$, where $U^{(k)}$ is matrix U on the kth iteration of the main loop of the algorithm, defines a nondecreasing sequence of values $\{f[U^{(k)}]\}$. The algorithm terminates when the sequence $\{f[U^{(k)}]\}$ converges.

The strategy for choosing the pair of matrices to improve upon leads to different algorithms. The simplest one is a sweep of all possible pairs of matrices (hill climbing). An alternative strategy is to choose the pair that gives the biggest increase in the value of $f(U)$ (steepest-ascent hill climbing). Other techniques of heuristic search can be applied, too. We used the hill-climbing search for the numerical tests presented in Section 3.

We have no rigorous convergence proof, and we do not know whether the maximum reached is global or whether the global maximum is unique. We plan to consider some of these questions, along with related topics, in a separate paper.

APPENDIX B: MAXIMIZING $F(U)$ (SINGLE-MATRIX CASE)

Let $\lambda(A)$ be the vector of the eigenvalues of an $n \times n$ real symmetric matrix A such that

$$\lambda_1(A) \geq \ldots \geq \lambda_n(A).$$

Lemma 1. Let Q be an $n \times n$ unitary matrix with $Q = [q_1, \ldots, q_n]$. For any r such that $1 \leq r \leq n$ define $Q_r = [q_1, \ldots, q_r]$. For any $n \times n$ symmetric matrix A the following inequality holds:

$$\sum_{i=1}^{r} q_i{}^T A q_i = \mathrm{tr}(Q_r{}^T A Q_r) \leq \sum_{i=1}^{r} \lambda_i(A).$$

Proof: Let $A^{(r)} = Q_r{}^T A Q_r$. From the interlacing property (corollary 8.1.4 in Ref. 21) for any k,

$$\begin{aligned} \lambda_{k+1}[A^{(k+1)}] \leq \lambda_k[A^{(k)}] \leq \lambda_k[A^{(k+1)}] \leq \ldots \leq \lambda_1[A^{(k)}] \\ \leq \lambda_1[A^{(k+1)}]. \end{aligned}$$

By induction we infer that

$$\lambda_r[A^{(r)}] \leq \lambda_r[A^{(n)}], \ldots, \lambda_1[A^{(r)}] \leq \lambda_1[A^{(n)}].$$

Therefore $\mathrm{tr}[A^{(r)}] = \lambda_r[A^{(r)}] + \ldots + \lambda_1[A^{(r)}] \leq \Sigma_{i=1}^{r} \lambda_i(A)$. ■

Theorem 1. Given an $n \times n$ real symmetric matrix $\mathcal{M}$,

$$\begin{aligned} \max_{U \text{ unitary}} f(U) &= \max_{U \text{ unitary}} \sum_{i=1}^{n} \max\{(U^T \mathcal{M} U)_{ii}, 0\} \\ &= \sum_{\lambda_i(\mathcal{M})>0} \lambda_i(\mathcal{M}). \end{aligned} \tag{B1}$$

Proof: When U is the matrix of the eigenvectors of $\mathcal{M}$, we obviously achieve the value defined in Eq. (B1).

We will show that for any U

$$\sum_{i=1}^{n} \max\{(U^T \mathcal{M} U)_{ii}, 0\} \leq \sum_{\lambda_i(\mathcal{M})>0} \lambda_i(\mathcal{M}).$$

Without loss of generality assume that the first r diagonal entries of $U^T \mathcal{M} U$ are positive; then, using lemma 1, we get

$$\begin{aligned} \sum_{i=1}^{r} (U^T \mathcal{M} U)_{ii} = \mathrm{tr}(U_r{}^T \mathcal{M} U_r) \leq \sum_{i=1}^{r} \lambda_i(\mathcal{M}) \\ \leq \sum_{\lambda_i(\mathcal{M})>0} \lambda_i(\mathcal{M}), \end{aligned}$$

where U_r is the matrix consisting of the first r columns of U. ■

ACKNOWLEDGMENT

Brent L. Ellerbroek and Robert J. Plemmons acknowledge support from the U.S. Air Force Office of Scientific Research.

REFERENCES AND NOTES

1. R. Q. Fugate, D. L. Fried, G. A. Ameer, B. R. Boeke, S. L. Browne, P. H. Roberts, R. E. Ruane, G. A. Tyler, and L. M. Wopat, "Measurement of atmospheric wave-front distortion using scattered light from a laser guide-star," Nature (London) **353,** 144–146 (1991).
2. F. Roddier, M. Northcott, and J. E. Graves, "A simple low-order adaptive optics system for near-infrared applications," Publ. Astron. Soc. Pac. **103,** 131–149 (1991).
3. R. Q. Fugate, B. L. Ellerbroek, C. H. Higgins, M. P. Jelonek, W. J. Lange, A. C. Slavin, W. J. Wild, D. M. Winker, J. M. Wynia, J. M. Spinhirne, B. R. Boeke, R. E. Ruane, J. F. Moroney, M. D. Oliker, D. W. Swindle, and R. A. Cleis, "Two generations of laser-guide-star adaptive-optics experiments at the Starfire Optical Range," J. Opt. Soc. Am. A **11,** 310–324 (1994).
4. V. E. Zuez and V. P. Lukin, "Dynamic characteristics of optical adaptive systems," Appl. Opt. **26,** 139–144 (1987).
5. C. Boyer, E. Gendron, and P. Y. Madec, "Adaptive optics for high resolution imagery: control algorithms for optimized modal corrections," in *Lens and Optical Systems Design*, H. Zuegge, ed., Proc. Soc. Photo-Opt. Instrum. Eng. **1780,** 943–957 (1992).
6. E. Gendron, "Modal control optimization in an adaptive optics system," presented at the International Commission for Optics–16 Satellite Conference, August 2–5, 1993, Garching, Germany.
7. C. Schwartz, G. Baum, and E. N. Ribak, "Turbulence-degraded wave fronts as fractal surfaces," J. Opt. Soc. Am. A **11,** 444–451 (1994).
8. G. Rousset, J. C. Fontanella, P. Kern, P. Gigan, F. Rigaut, P. Lena, C. Boyer, P. Jagourel, J. P. Gaffard, and F. Merkle, "First diffraction limited astronomical images with adaptive optics," Astron. Astrophys. **230,** L29–L32 (1990).
9. G. Rousset, J. L. Beuzit, N. Hubin, E. Gendron, C. Boyer, P. Y. Madec, P. Gigan, J. C. Richard, M. Vittot, J. P. Gaffard, F. Rigaut, and P. Lena, "The Come-On-Plus adaptive optics system: results and performance," presented at the International Commission for Optics–16 Satellite Conference, August 2–5, 1993, Garching, Germany.
10. F. Rigaut, G. Rousset, P. Kern, J. C. Fontanella, J. P. Gaffard, F. Merkle, and P. Lena, "Adaptive optics on the 3.6 m telescope: results and performance," Astron. Astrophys. **250,** 280–290 (1991).
11. G. Rousset, J. Fontanella, P. Kern, P. J. Lena, P. Gigan, F. Rigaut, J. Gaffard, C. Boyer, P. Jagourel, and F. Merkle, "Adaptive optics prototype system for infrared astronomy," in *Amplitude and Intensity Spatial Interferometry*, J. B. Breckinridge, ed., Proc. Soc. Photo-Opt. Instrum. Eng. **1237,** 336–344, 1990.
12. E. Gendron, J. Cuby, F. Rigaut, P. J. Lena, J. Fontanella, G. Rousset, J. Gaffard, C. Boyer, J. Richard, M. Vittot, F. Merkle, and N. Hubin, "Come-On-Plus project: an upgrade of the Come-On adaptive optics prototype system," in *Active and Adaptive Optical Systems*, M. A. Ealey, ed., Proc. Soc. Photo-Opt. Instrum. Eng. **1542,** 297–307 (1991).
13. F. Roddier, M. J. Northcott, J. E. Graves, D. L. McKenna, and D. Roddier, "One-dimensional spectra of turbulence-induced Zernike aberrations: time-delay and isoplanicity error in partial adaptive compensation," J. Opt. Soc. Am. A **10,** 957–965 (1993).
14. R. R. Parenti and R. J. Sasiela, "Laser-guide-star systems for astronomical applications," J. Opt. Soc. Am. A **11,** 288–309 1994.
15. D. L. Fried, "Least-squares fitting a wave-front distortion estimate to an array of phase difference measurements," J. Opt. Soc. Am. **67,** 370–375 (1977).
16. R. H. Hudgin, "Wave-front reconstruction for compensated imaging," J. Opt. Soc. Am. **67,** 375–378 (1977).
17. J. Herrmann, "Least-squares wave-front errors of minimum norm," J. Opt. Soc. Am. **70,** 28–35 (1980).
18. D. P. Greenwood and D. L. Fried, "Power spectra requirements for wave-front compensation systems," J. Opt. Soc. Am. **66,** 193–206 (1976).
19. J. Y. Wang and J. K. Markey, "Modal compensation of atmospheric turbulence phase distortion," J. Opt. Soc. Am. **68,** 78–87 (1978).
20. R. J. Noll, "Zernike polynomials and atmospheric turbulence," J. Opt. Soc. Am. **66,** 207–211 (1976).
21. G. H. Golub and C. Van Loan, *Matrix Computations*, 2nd ed. (Johns Hopkins U. Press, Baltimore, Md., 1989).
22. B. L. Ellerbroek, "First-order performance evaluation of adaptive-optics systems for atmospheric-turbulence compensation in extended-field-of-view astronomical telescopes," J. Opt. Soc. Am. A **11,** 783–805 (1994).
23. E. P. Wallner, "Optimal wave-front correction using slope measurements," J. Opt. Soc. Am. **73,** 1771–1776 (1983).
24. B. M. Welsh and C. S. Gardner, "Effects of turbulence-induced anisoplanatism on the imaging performance of adaptive-astronomical telescopes using laser guide stars," J. Opt. Soc. Am. A **8,** 69–80 (1991).
25. R. C. Fisher, *An Introduction to Linear Algebra* (Dickenson, Encino, Calif., 1970).
26. Equation (2.27) requires that the matrix S be positive definite. S is positive semidefinite by construction, and any eigenvector of S with a zero eigenvalue defines a wave-front-sensor measurement mode that must be identically zero. Such measurement modes, in the cases in which they exist at all, cannot contribute to the wave-front estimate. When necessary we may replace the measurement vector $\mathbf{s}$ by its projection onto the subspace orthogonal to all such modes and redefine M and G as their restrictions to this subspace.
27. G. A. Tyler, "Turbulence-induced adaptive-optics performance evaluation: degradation in the time domain," J. Opt. Soc. Am. A **1,** 251–262 (1984).
28. The case of a fixed, known wind direction requires a slight modification to the formulas developed in Ref. 22 for the matrices A and S. Ensemble averaging over the direction of the wind in Eq. (3.22) of Ref. 22 now has no effect, and the ray separation vector $\boldsymbol{\Delta}$ must be replaced by $\boldsymbol{\Delta} + (\tau_1 - \tau_2)\mathbf{v}$ for the remainder of the derivation. The velocity v of the random wind must also be set to zero. The resulting formula for a general element of the matrix A or S is identical to Eq. (3.27) of Ref. 22, except that the term $f(2\delta v/D, 2\Delta/D)$ is replaced by $f(0, 2|\delta\mathbf{v} + \boldsymbol{\Delta}|/D)$. The function $f(a, b)$ remains as defined by Eq. (3.28) of Ref. 22.